



HAL
open science

A detailed characterisation study of Li₆PS₅Cl ionic conductors from several synthetic routes

Mathieu Morcrette, Xavier Randrema, Cedric Barcha, Mohamed Chakir,
Virginie Viallet

► **To cite this version:**

Mathieu Morcrette, Xavier Randrema, Cedric Barcha, Mohamed Chakir, Virginie Viallet. A detailed characterisation study of Li₆PS₅Cl ionic conductors from several synthetic routes. *Solid State Sciences*, 2021, 118, 10.1016/j.solidstatesciences.2021.106681 . hal-03611424

HAL Id: hal-03611424

<https://u-picardie.hal.science/hal-03611424>

Submitted on 2 Aug 2023

HAL is a multi-disciplinary open access archive for the deposit and dissemination of scientific research documents, whether they are published or not. The documents may come from teaching and research institutions in France or abroad, or from public or private research centers.

L'archive ouverte pluridisciplinaire **HAL**, est destinée au dépôt et à la diffusion de documents scientifiques de niveau recherche, publiés ou non, émanant des établissements d'enseignement et de recherche français ou étrangers, des laboratoires publics ou privés.



Distributed under a Creative Commons Attribution - NonCommercial 4.0 International License

A detailed characterisation study of Argyrodite ionic conductors from several synthetic routes.

Xavier Randrema^{1,2,3}, Cédric Barcha^{1,2,3}, Mohamed Chakir¹, Virginie Viallet^{2,3} and Mathieu Morcrette^{2,3}

¹ Renault Technocentre, 1 avenue du Golf, 78084 Guyancourt, France

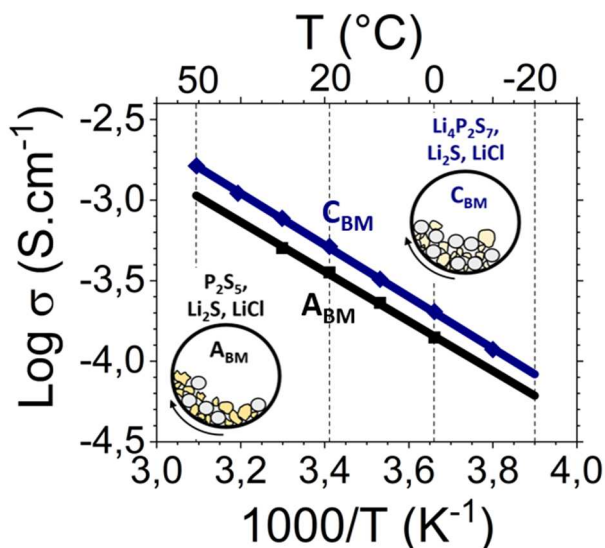
² Laboratoire de Réactivité et Chimie des Solides (LRCS), UMR CNRS 7314, Université de Picardie Jules Verne, HUB de l'Energie, 15 Rue Baudelocque, 80039 Amiens, France

³ Réseau sur le Stockage Electrochimique de l'Energie (RS2E), FR CNRS 3459, France

E-mail: mathieu.morcrette@u-picardie.fr

Abstract

Studies of argyrodite $\text{Li}_6\text{PS}_5\text{Cl}$ as solid electrolyte are increasing, motivated by its high ionic conductivity and its easy processability. However, development of All-Solid-State-Batteries lies on the ability to produce such compound with a good purity. This work presents the characterization results of different argyrodite grades: commercial and homemade one. In parallel, synthesis of $\text{Li}_6\text{PS}_5\text{Cl}$ from $\text{Li}_4\text{P}_2\text{S}_7$ precursor is reported for the first time. The purity effect on these properties will be explored by using X-ray diffraction coupled with Raman spectroscopy and electrochemical impedance spectroscopy technics. Crystal properties investigations will be particularly conducted, given that smaller crystallite sizes would lead to an enhanced ionic percolation network by increasing the microstructure homogeneity in catholyte. Such SE could be obtained only by avoiding a *post* synthesis annealing treatment. Finally, electrochemical properties of the different reported grades will also be discussed in this study. We demonstrate here 1. the beneficial effect of $\text{Li}_4\text{P}_2\text{S}_7$ to obtain a pure sulfur-based solid electrolyte with nanometric crystallites without solid state synthesis and 2. the impact of impurities on its ionic and electrochemical properties.



Keywords: Solid State Battery; Solid Electrolyte; Argyrodite; $\text{Li}_6\text{PS}_5\text{Cl}$; Ionic conductivity; Mecanosynthesis

1. Introduction

Lithium secondary batteries have been widely used to provide power sources in electronic devices since its commercialization by Sony in 1991. Recently, higher energy density and longer cycle performance are required, mostly to target Electric Vehicles (EV) market to decrease our fossil energy dependence. However, there are safety concerns due to the flammability of liquid electrolytes^{1,2}. To address the problem, scientific community tried to move on All-Solid-State-Batteries (ASSB), meaning the replacement of liquid electrolyte by solid electrolyte (SE), able to play both electronic insulating separator and ionic conductor. This trend is clearly observable in publications number concerning two classes of SE: polymer³ and inorganic⁴ families. The second category has attracted material scientists since the early 20th century and can also be divided in two parts: oxide and sulfide. Oxide SE can be handled at room atmosphere but have lower conductivity. They need high temperature for processing so as to get fully dense layers⁵. Sulfide SE present higher ionic conductivity but are reacting with room atmosphere moisture, they are ductile so they can be compacted at room temperature with moderate external pressure⁶. As an example of impressive conductivity, LGPS showed a value of 12 mS.cm⁻¹ at room temperature⁷, creating a huge interest in sulfide SE since 2011. Since then, several phases based on the binary Li₂S-P₂S₅ system were studied⁸, so as to improve ionic conductivities. Moreover, several studies targeted to define the electrochemical stability of common SE. By DFT calculations^{9,10}, electrochemical windows seem to be extremely restrained, especially for sulfides SE.

In this work, a promising sulfide based solid electrolyte, Li₆PS₅Cl, will be studied. The high ionic conductivity¹¹ presented by this phase makes it a competitive candidate for upscaling and industrial purpose¹². Many proofs of Li₆PS₅Cl efficiency in ASSB were shown, both in dry^{13,14} and wet process^{15,16} assembly. Nevertheless, one of the limitations of ASSB development is the ability to produce at larger scale Li₆PS₅Cl with decent purity. Despite the low quantity produced by most of the publications, most of them have reported Li₆PS₅Cl phase with several impurities^{14,13,17} such as Li₂S, and LiCl precursors after ball milling process. To improve the resulting phase purity and crystallinity, an additional annealing treatment step at 550 °C is commonly added¹⁸.

In this present study, by systematic X-ray diffraction coupled with Raman and electrochemical impedance spectroscopy, we will focus on 2 commercial argyrodite grades, in addition to our grade obtained by conventional mecano-synthesis. To increase the purity of the product, hepta-pyro-thiophosphate (Li₄P₂S₇) precursor will be synthesized for the first time and a

new mechanochemical synthesis route will be proposed, leading to higher ionic conductivity of the resulting Li₆PS₅Cl. Finally, effect of SE's purity on the electrochemical window will be investigated.

2. Experimental Section

2.1. Preparation of Materials. Homemade Li₆PS₅Cl (**sample A_{BM}**) was prepared by mecano-synthesis route from Li₂S (Sigma Aldrich 99%), P₂S₅ (Sigma Aldrich 99%) and LiCl (Acros Organic 99%) precursors mixed in stoichiometric proportions. The mechanical milling treatment was carried out for 1 g overall mass of mixed powders with 15 zirconia balls (ϕ10 mm, overall mass = 30 g) in a zirconia jar (45 mL). The ball milling was done with a Pulverisette 7 instrument at 600 rpm for 10 h. Subsequently, the powder was annealed for 5 h at 550 °C in a hermetic stainless-steel reactor sealed with a copper ring (**sample A**). For the new mechanochemical reaction route, Li₄P₂S₇ was first obtained by mechanical milling of Li₂S (Sigma Aldrich 99%) and P₂S₅ (Sigma Aldrich 99%) in stoichiometric proportions for 1 g overall mass of mixed powders with 6 zirconia balls (ϕ10 mm, overall mass = 12 g) in a zirconia jar (45 mL) using a Pulverisette 7 instrument at 600 rpm for 10 h. The synthesis of Li₆PS₅Cl (**sample C**) was then prepared by mecano-synthesis method between Li₄P₂S₇, Li₂S (Sigma Aldrich 99%) and LiCl (Acros Organic 99%) in stoichiometric proportions for 1 g overall mass of mixed powders with 15 zirconia balls (ϕ10 mm, overall mass = 12 g) in a zirconia jar (45 mL) using a Pulverisette 7 instrument at 600 rpm for 10 h. The commercial grades of Li₆PS₅Cl were purchased from Ampcera (**sample B_{Ampcera}**) and NEI (**sample B_{NEI}**).

2.2. Material Characterization. Crystallographic phase identification was performed using a Bruker D8 Advanced diffractometer with Cu radiation ($\lambda_1 = 1.54056 \text{ \AA}$, $\lambda_2 = 1.54439 \text{ \AA}$). Diffraction patterns were refined by Le Bail method using Fullprof software. Stainless steel in-situ cell with beryllium window¹⁹ was used to prevent sample to be exposed to air. Raman spectroscopy was performed using a DXR3 Raman Microscope from Thermo Fisher with a 532 nm excitation source and a laser power of 1 mW. Peak deconvolution was processed using the Omnic software with a Voigt function. Electrochemical impedance spectroscopy (EIS) was used to evaluate the SE ionic conductivity as function of temperature, in the range of 0.1 Hz to 30 MHz by using MTZ-35 impedance analyser from Biologic. Signal amplitude was fixed at 50 mV. The measurements were conducted with 10 mm diameter pellet pressed at 625 MPa (5 tons), by cold pressing in glove box under argon. Pellet compacity reached a value close to 85 %. Electrochemical window was evaluated by galvanostatic cycles at Room Temperature (RT) with a VMP3 equipment from Biologic.

Voltage limits were settled between 0 - 2 V vs Li⁺/Li for reduction reaction and 2 - 5 V vs Li⁺/Li for oxidation reaction with a current density intentionally fixed to a low value (15 $\mu\text{A}\cdot\text{cm}^{-1}$). The pseudo-battery assembled in pellet of 10 mm diameter (*cf.* Supporting Information) was based on 80 mg of Li₆PS₅Cl pressed at 125 MPa, then 10 mg of catholyte composed of Li₆PS₅Cl:C45 (7:3) pressed at 375 MPa and a counter electrode composed of Li_{0.5}In²⁰.

3. Results and discussion

3.1. Comparison between Li₆PS₅Cl grades. Figure 1 shows X-ray diffraction (XRD) patterns and profile matching refinement of the different grades of Li₆PS₅Cl. Although main reflections can be indexed for all patterns with the face-centred cubic structure (space group $F\bar{4}3m$ ^{21,22}), several samples present precursors remains such as Li₂S precursor observed in XRD pattern, at $2\theta = 27^\circ$, for A_{BM}, A and B_{Ampcera} samples. For A_{BM} sample especially, both precursors Li₂S and LiCl are highly visible leading to the assumption that the chemical reaction involving Li₂S, LiCl and P₂S₅ is not complete as reported in previous publications^{13,17}. In A sample, no impurities phases are detected, confirming the beneficial effect of the heat treatment step²³.

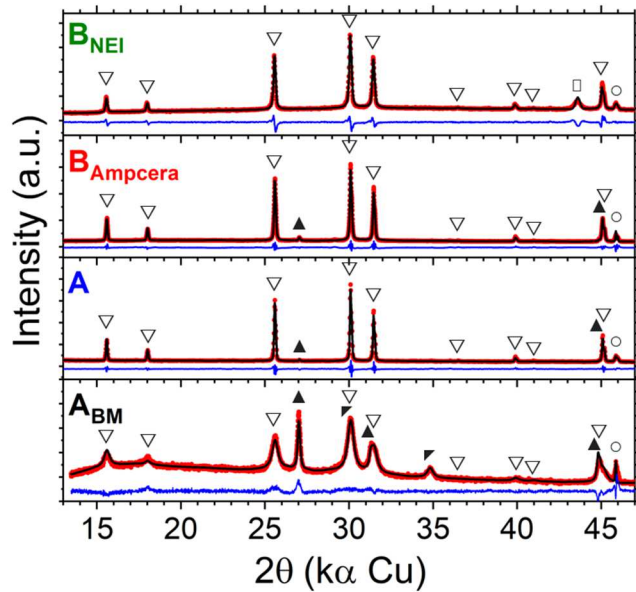


Figure 1 : Profile matching of Li₆PS₅Cl grades. Conventional mecosynthesis (sample A_{BM}), conventional mecosynthesis followed by annealing at 550 °C (sample A), commercial Ampcera powder (sample B_{Ampcera}) and commercial NEI powder (sample B_{NEI}). Bragg positions are represented with Li₆PS₅Cl (∇), Li₂S (\blacktriangle), LiCl (\square), Fe (\circ) and Be (\square).

To extract the crystallite size from previous refinement, NIST standard (LaB₆-Si powder) was used to access to the diffractometer resolution (*cf.* Supporting Information). The **Table 1** below presents both cubic lattice parameter *a* and crystallite size for each sample. Interestingly, A_{BM} sample

presents nano-crystallites, but the solid-state synthesis through the annealing treatment leads to an important growth of the crystals as shown by the value for A sample. This could be problematic in catholyte electrode formulated by dry process, as we require small SE's particles to improve the microstructure homogeneity and so the ionic percolation network. An appropriate balance must be struck, by considering the phase purity and the ionic conductivity on one side and by trying to limit employment of a *post* synthesis annealing treatment to keep small crystallite sizes on the other side. Concerning commercial grades, we observe high crystallite sizes especially for B_{Ampcera} sample, suggesting that a temperature step is performed during or after the synthesis.

Table 1 : Information obtained for sample A_{BM} (mecanosynthesis), A (annealing at 550 °C after mecosynthesis), B_{Ampcera} and B_{NEI} from refinement by the Le Bail method.

Sample	Lattice parameter (Å)	Crystallite size (nm)
A _{BM}	9,8406 (5)	15
A	9,8444 (2)	161
B _{Ampcera}	9,8433 (2)	118
B _{NEI}	9,8530 (2)	62

Figure 2 reminds the majors units visible by Raman spectroscopy. Given the complexity to obtain pure thiophosphate-based SE, we also present here polyhedra obtained in the case of the Li₂S-P₂S₅ binary system⁸.

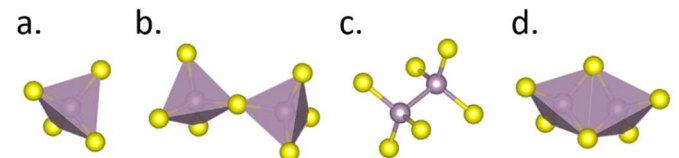


Figure 2 : Main anionic polyhedra in Li₆PS₅Cl or Li₂S-P₂S₅ based SE with a. ortho-thiophosphate units (PS₄³⁻), pyro-thiodiphosphate (P₂S₇⁴⁻), c. hypo-thiophosphate (P₂S₆⁴⁻) and d. metha-thiodiphosphate (P₂S₆²⁻). Sulfur atoms are presented in yellow and phosphorous atoms in grey.

Figure 3a shows Raman spectrum of each sample in the area of interest of ortho-thiophosphate units PS₄³⁻, which are isolated units in Li₆PS₅Cl face-centred cubic structure. Their expected principal Raman bands (stretching vibration mode ν_s) are at 425 cm^{-1} with two bands of lower intensities at 199 cm^{-1} and 573 cm^{-1} , and another band associated to a bending vibration mode δ at 272 cm^{-1} ²⁴. Nevertheless, sample B_{NEI} presents an impurity around 480 cm^{-1} previously reported as S-S vibration in S₈²⁴. Moreover, it is possible to extract accurate information about the presence of other P_xS_y units

between 370 cm^{-1} and 450 cm^{-1} ²⁵ and **Figure 3b** presents peak deconvolution of each sample in this range. Interestingly, A_{BM} sample shows an impurity centred at 405 cm^{-1} known as pyro-thiophosphate units ($\text{P}_2\text{S}_7^{4-}$)²⁶ which is the base for the amorphous network of $\text{Li}_4\text{P}_2\text{S}_7$ ⁸. Thus, this confirms the idea of an incomplete reaction as suggested previously, leading to the presence of $\text{Li}_4\text{P}_2\text{S}_7$, LiCl and Li_2S in the powder obtained by ball milling only. Concerning the annealed sample and both commercial grades, only PS_4^{3-} are visible after the band deconvolution.

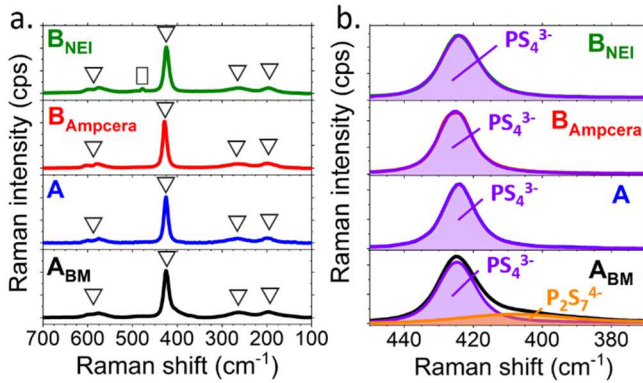


Figure 3 : Raman spectra of $\text{Li}_6\text{PS}_5\text{Cl}$ grades. Conventional mecosynthesis (sample A_{BM}), conventional mecosynthesis followed by annealing at 550 $^\circ\text{C}$ (sample A), commercial Ampcera powder (sample B_{Ampcera}) and commercial NEI powder (sample B_{NEI}) with a. area of interest of thiophosphates with PS_4^{3-} (∇) and S_8 (\square) and b. peak deconvolution between 370 cm^{-1} and 450 cm^{-1} showing the bands of PS_4^{3-} (purple) and $\text{P}_2\text{S}_7^{4-}$ units (orange).

Figure 4a shows the Nyquist plot of each sample at 20 $^\circ\text{C}$. The semi-circles attest the presence of only one ionic contribution. **Figure 4b** presents the resulting Arrhenius plot based on the linear regression of experimental data between 50 $^\circ\text{C}$ and -20 $^\circ\text{C}$. Impact of annealing treatment is clearly noticeable from A_{BM} to A samples, meaning controlling the purity of $\text{Li}_6\text{PS}_5\text{Cl}$ is a vital step that influence drastically the resulting ionic conductivity. A surprising result here is the conductivity of B_{NEI} and particularly its activation energy (E_a). The behaviour is completely different from other $\text{Li}_6\text{PS}_5\text{Cl}$ grades, with higher ionic conductivity at high temperature. The presence of S_8 could be at the origin of this particular behaviour and will be investigated in part 3.2.

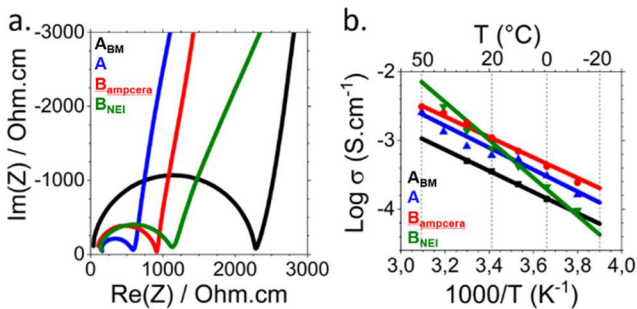


Figure 4 : Ionic conductivities of each sample with a. Nyquist plot at 20 $^\circ\text{C}$ and b. Arrhenius plot from the linear regression of experimental data.

To have an overview of the complete data set, **Table 2** below presents both ionic conductivities average at 20 $^\circ\text{C}$ and E_a for each sample.

Table 2 : Ionic conductivities (σ_i) at 20 $^\circ\text{C}$ and activation energies (E_a) of A_{BM} , A, B_{Ampcera} and B_{NEI} samples.

Sample	Compacity (%)	σ_i at 20 $^\circ\text{C}$ (S.cm^{-1})	E_a (eV)
A_{BM}	81	3.5×10^{-4}	0.19
A	80	6.0×10^{-4}	0.19
B_{Ampcera}	88	1.1×10^{-3}	0.18
B_{NEI}	81	9.6×10^{-4}	0.33

3.2. Purity and ionic conductivity. To confirm the link between product purity and ionic conductivity, the particular case of sample B_{NEI} was studied according to Raman spectroscopy results, which highlighted the presence of S_8 impurity. After heat treatment at 130 $^\circ\text{C}$ for 10 h under vacuum, Raman spectrum of B_{NEI} showed a pure phase (S_8 evaporation temperature is 115 $^\circ\text{C}$), as presented in **Figure 5a**. **Figure 5b** presents the resulting Arrhenius plot with a conventional value of E_a equivalent to 0,21 eV, slightly superior to previous study²⁷.

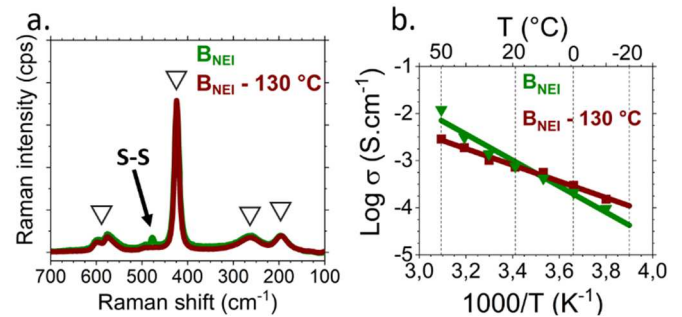


Figure 5 : Study of B_{NEI} before (green) and after treatment at 130 $^\circ\text{C}$ (brown) with a. Raman spectrum with PS_4^{3-} units (∇) and S_8 at 480 cm^{-1} and b. Arrhenius plot from the linear regression of experimental data.

This result shows the relationship existing between the phase purity and its ionic conductivity. For the development of large-scale synthesis, it is mandatory to carefully control the synthesis stages, with or without a *post* annealing treatment.

3.3. New synthesis route using $\text{Li}_4\text{P}_2\text{S}_7$. According to the incomplete reaction showed for A_{BM} sample along with impurities, a new synthesis of $\text{Li}_6\text{PS}_5\text{Cl}$ is proposed through $\text{Li}_4\text{P}_2\text{S}_7$ precursor. First, the synthesis of $\text{Li}_4\text{P}_2\text{S}_7$ was

conducted by ball milling of Li_2S and P_2S_5 according to the following reaction:

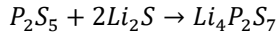


Figure 6 presents the Raman spectrum of the resulting powder with a peak deconvolution between 360 and 450 cm^{-1} showing the presence of PS_4^{3-} , $\text{P}_2\text{S}_7^{4-}$ and $\text{P}_2\text{S}_6^{4-}$ units. The presence $\text{P}_2\text{S}_7^{4-}$ units confirmed that some $\text{Li}_4\text{P}_2\text{S}_7$ was successfully synthesized. XRD and EIS at RT are presented in Supporting Information and attest the presence of an amorphous phase which is expected for $\text{Li}_4\text{P}_2\text{S}_7$ obtained by ball-milling⁸, and a conductivity of $4.4 \times 10^{-5} \text{ S.cm}^{-1}$ consistent with the one assumed by Dietrich *et al.*²⁵.

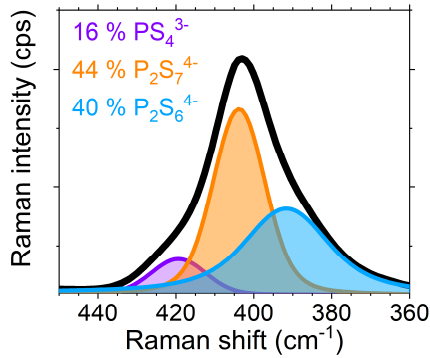


Figure 6 : Raman spectrum of $\text{Li}_4\text{P}_2\text{S}_7$ obtained by the new mecanosynthesis method. Peak deconvolution between 370 cm^{-1} and 450 cm^{-1} with PS_4^{3-} units (purple), $\text{P}_2\text{S}_7^{4-}$ units (orange) and $\text{P}_2\text{S}_6^{4-}$ units (cyan).

Secondly, the synthesis of $\text{Li}_6\text{PS}_5\text{Cl}$ was performed by the following reaction:

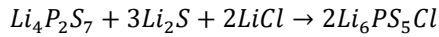


Figure 7 presents XRD patterns and profil matching refinements of the resulting powder after ball-milling (C sample). This sample shows $\text{Li}_6\text{PS}_5\text{Cl}$ structure with small crystallite size as suggested by peaks broadening. This size was evaluated to be around 12 nm, comparable to the one obtained for A_{BM} sample. Thus, the synthesis through $\text{Li}_4\text{P}_2\text{S}_7$ leads to higher purity argyrodite compound with a similar crystallite size compared to the classical reaction between Li_2S , P_2S_5 and LiCl .

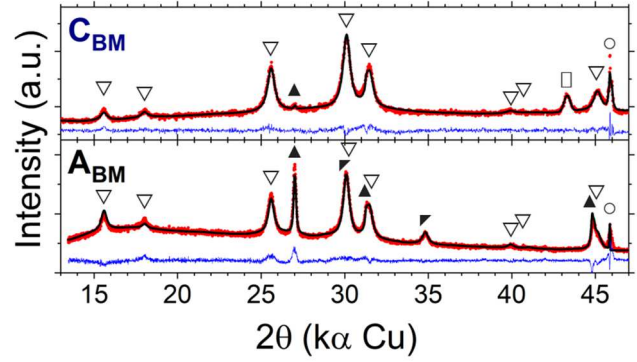


Figure 7 : Profile matching of $\text{Li}_6\text{PS}_5\text{Cl}$ grades. Remind of conventional mecanosynthesis (sample A_{BM}) and synthesis from $\text{Li}_4\text{P}_2\text{S}_7$ precursor (sample C_{BM}). Bragg positions for $\text{Li}_6\text{PS}_5\text{Cl}$ (∇), Li_2S (\blacktriangle), LiCl (\square), Fe (\circ) and Be (\diamond).

Figure 8a presents Raman spectrum of sample C. Compared to A_{BM} sample, we can conclude that the powder purity was improved because only PS_4^{3-} vibrations are observed. **Figure 8b** shows the Arrhenius plot of both A_{BM} and C_{BM} samples with an interesting enhancement of the ionic conductivity by a factor 5. This highlights the relationship between the impact of synthesis and the phase purity, correlated with the resulting ionic conductivity, which is higher for the new route mecanosynthesis.

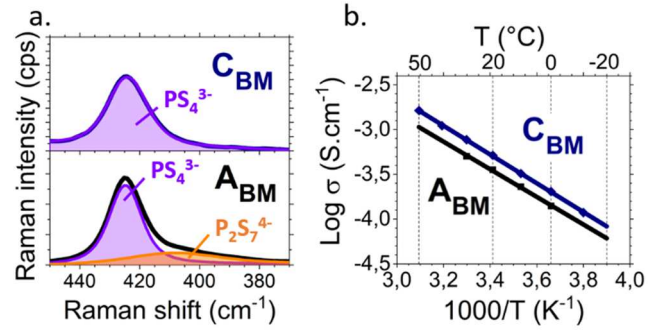


Figure 8 : Raman spectrum and Arrhenius plot of C_{BM} (dark blue) and A_{BM} (black) with a. the peak deconvolution between 370 cm^{-1} and 450 cm^{-1} with PS_4^{3-} (purple) and $\text{P}_2\text{S}_7^{4-}$ units (orange) and b. Arrhenius plot from the linear regression of experimental data.

3.4. Electrochemical stability. All samples were evaluated in pseudo-battery system²⁸⁻³⁰ in order to study the impact of powder purity on their electrochemical window stability. SE powders were used as active material and mixed with C45 in a ratio of 7:3. The reduction and oxidation reactions of $\text{Li}_6\text{PS}_5\text{Cl}$, involving respectively 798 mAh.g^{-1} and 499 mAh.g^{-1} ³⁰ are shown below:

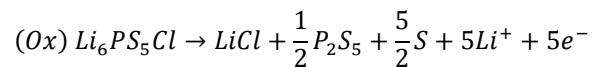
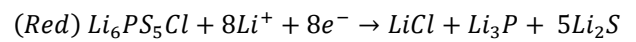


Figure 9a and **Figure 9b** present the reduction and oxidation studies of the different samples. First, we can clearly observe

the difference of capacities between reduction and oxidation reactions, respectively more than 200 mAh.g^{-1} and around 3 mAh.g^{-1} . Secondly, all samples allowed the oxidation or reduction on the first step (charge or discharge) of the galvanostatic cycles. We think that these samples are not stables and they decompose. Indeed, we assist to the reduction of phosphorous around 1 V vs Li^+/Li during the first discharge, as showed in literature³⁰. Concerning reduction capacity values, A_{BM} shows the higher one (469 mAh.g^{-1}) followed by C_{BM} (425 mAh.g^{-1}), B_{Ampcera} (300 mAh.g^{-1}), B_{NEI} (312 mAh.g^{-1}) and A (180 mAh.g^{-1}). According to these results, it seems that the capacity is not linked to $\text{Li}_6\text{PS}_5\text{Cl}$ degradation but rather to the presence of $\text{Li}_4\text{P}_2\text{S}_7$ impurities, as A sample does not contain amorphous phase after annealing treatment at 550°C .

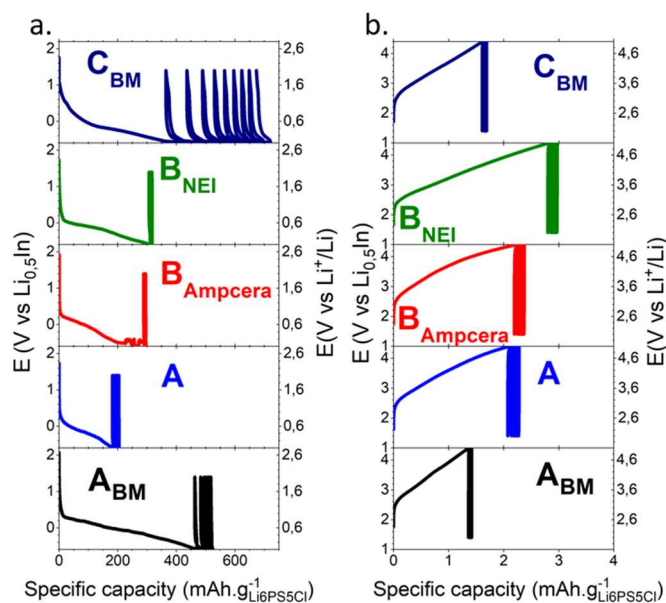


Figure 9 : Galvanostatic cycles comparison between A_{BM} (black), A (blue), B_{Ampcera} (red), B_{NEI} (green) and C_{BM} (dark blue) with a. reduction study between $0 - 2 \text{ V}$ vs Li^+/Li and b. oxidation study between $2 - 5 \text{ V}$ vs Li^+/Li .

To identify accurately the electrochemical window, the derivative curves of every 1st cycle were plotted (*cf.* Supporting Information). It appears that voltage limits are contained within the range of 1 V to $2,7 \text{ V}$ vs Li^+/Li , $\pm 100 \text{ mV}$ according to the sample. This is in good agreement with the literature even if the oxidation potential was reported a little bit lower ($2,4 \text{ V}$ vs Li^+/Li)²⁸ but this may be linked to the different morphologies and percentages of carbon additive in the catholyte.

4. Conclusions

The combination of XRD, Raman and EIS have allowed us to attest that the conventional mecanosynthesis based on Li_2S , P_2S_5 and LiCl mixture is not complete and the resulting

powder still contains the precursors along with an amorphous phase identify as $\text{Li}_4\text{P}_2\text{S}_7$. It was also shown the importance of the heat treatment at 550°C in order to complete the reaction by solid state synthesis, along with the drawback to increase crystallite sizes. To enhance the product purity right after ball milling in order to keep the nanometric size of the electrolyte, the synthesis of $\text{Li}_6\text{PS}_5\text{Cl}$ was modified with the proposition of a new synthetic route using $\text{Li}_4\text{P}_2\text{S}_7$ precursor. The synthesis of $\text{Li}_4\text{P}_2\text{S}_7$ was conducted and the resulting powder showed amorphous phase by XRD, with the presence of $\text{P}_2\text{S}_7^{4-}$ units by Raman. The subsequent ball milling step of $\text{Li}_4\text{P}_2\text{S}_7$ with Li_2S and LiCl leads to pure $\text{Li}_6\text{PS}_5\text{Cl}$ as confirmed by XRD and Raman spectroscopy. The effect of phase purity was thus correlated to the ionic conductivity with the conclusion that synthesis optimization still need to be studied, to decrease side product presence which have a negative effect on the ionic conductivity. Indeed, compounds such as Li_2S and LiCl are insulators and it is mandatory to avoid them in SE, especially if fast-charge applications are targeted. Finally, the correlation between phase purity and electrochemical window did not seem to exist but we still observed that degradation capacities were higher for grades with lower purity. With those informations, we are insisting here on the viability of ASSB technology based on sulfide SE, which could be only unlocked by a consequent work on positive active materials and lithium metal protection.

Supporting Information

Supporting Information is available.

Acknowledgements

X. Randrema and C. Barcha are grateful to ANRT for partially supporting the funding of this research work between LRCS and Renault (CIFRE n°2018/0063 and n°2018/0657). U. Kudu is gladly thanked for discussions on the $\text{Li}_2\text{S}-\text{P}_2\text{S}_5$ system.

References

1. Goodenough, J. B. & Kim, Y. Challenges for Rechargeable Li Batteries. *Chem. Mater.* **22**, 587–603 (2010).
2. Wang, Q. *et al.* Thermal runaway caused fire and explosion of lithium ion battery. *J. Power Sources* **208**, 210–224 (2012).
3. Heiska, J., Nisula, M. & Karppinen, M. Organic electrode materials with solid-state. *J. Mater. Chem. A* **7**, 18735–18758 (2019).
4. Famprikis, T., Canepa, P., Dawson, J. A., Islam, M. S. & Masquelier, C. Fundamentals of inorganic solid-state electrolytes for batteries. *Nat. Mater.* **18**, 1278–1291 (2019).
5. Jin, Y. *et al.* An intermediate temperature garnet-type solid electrolyte-based molten lithium battery for grid energy storage. *Nat. Energy* **3**, 732–738 (2018).
6. Lian, P. *et al.* Inorganic sulfide solid electrolytes for all-solid-state lithium secondary batteries. *J. Mater. Chem. A*

- 7, 20540–20557 (2019).
7. Kamaya, N. *et al.* A lithium superionic conductor. *Nat. Mater.* **10**, 682–686 (2011).
 8. Kudu, Ö. U. *et al.* A review of structural properties and synthesis methods of solid electrolyte materials in the $\text{Li}_2\text{S}-\text{P}_2\text{S}_5$ binary system. *J. Power Sources* **407**, 31–43 (2018).
 9. Chen, H. M., Maohua, C. & Adams, S. Stability and ionic mobility in argyrodite-related lithium-ion solid electrolytes. *Phys. Chem. Chem. Phys.* **17**, 16494–16506 (2015).
 10. Richards, W. D., Miara, L. J., Wang, Y., Kim, J. C. & Ceder, G. Interface Stability in Solid-State Batteries. *Chem. Mater.* **28**, 266–273 (2016).
 11. Boulineau, S., Courty, M., Tarascon, J. M. & Viallet, V. Mechanochemical synthesis of Li-argyrodite $\text{Li}_6\text{PS}_5\text{X}$ (X = Cl, Br, I) as sulfur-based solid electrolytes for all solid state batteries application. *Solid State Ionics* **221**, 1–5 (2012).
 12. Schnell, J. *et al.* All-solid-state lithium-ion and lithium metal batteries – paving the way to large-scale production. *J. Power Sources* **382**, 160–175 (2018).
 13. Yubuchi, S. *et al.* Preparation of high lithium-ion conducting $\text{Li}_6\text{PS}_5\text{Cl}$ solid electrolyte from ethanol solution for all-solid-state lithium batteries. *J. Power Sources* **293**, 941–945 (2015).
 14. Boulineau, S., Tarascon, J. M., Leriche, J.-B. & Viallet, V. Electrochemical properties of all-solid-state lithium secondary batteries using Li-argyrodite $\text{Li}_6\text{PS}_5\text{Cl}$ as solid electrolyte. *Solid State Ionics* **242**, 45–48 (2013).
 15. Zhang, J. *et al.* All-solid-state batteries with slurry coated $\text{LiNi}_{0.8}\text{Co}_{0.1}\text{Mn}_{0.1}\text{O}_2$ composite cathode and $\text{Li}_6\text{PS}_5\text{Cl}$ electrolyte: Effect of binder content. *J. Power Sources* **391**, 73–79 (2018).
 16. Park, K. H. *et al.* Design Strategies, Practical Considerations, and New Solution Processes of Sulfide Solid Electrolytes for All-Solid-State Batteries. *Adv. Energy Mater.* **8**, 1–24 (2018).
 17. Ruhl, J., Riegger, L. M., Ghidui, M. & Zeier, W. G. Impact of Solvent Treatment of the Superionic Argyrodite $\text{Li}_6\text{PS}_5\text{Cl}$ on Solid-State Battery Performance. *Adv. Energy Sustain. Res.* **2000077**, 1–10 (2021).
 18. Wang, S. *et al.* High-Conductivity Argyrodite $\text{Li}_6\text{PS}_5\text{Cl}$ Solid Electrolytes Prepared via Optimized Sintering Processes for All-Solid-State Lithium–Sulfur Batteries. *ACS Appl. Mater. Interfaces* **10**, 42279–42285 (2018).
 19. Leriche, J. B. *et al.* An Electrochemical Cell for Operando Study of Lithium Batteries Using Synchrotron Radiation. *J. Electrochem. Soc.* **157**, A606 (2010).
 20. Webb, S. A., Baggetto, L., Bridges, C. A. & Veith, G. M. The electrochemical reactions of pure indium with Li and Na: Anomalous electrolyte decomposition, benefits of FEC additive, phase transitions and electrode performance. *J. Power Sources* **248**, 1105–1117 (2014).
 21. Chida, S. *et al.* Variation in structure and Li^+ -ion migration in argyrodite-type $\text{Li}_6\text{PS}_5\text{X}$ (X = Cl, Br, I) solid electrolytes. *J. Solid State Electrochem.* **1496**, 742–746 (2016).
 22. Yu, C., van Eijck, L., Ganapathy, S. & Wagemaker, M. Synthesis, structure and electrochemical performance of the argyrodite $\text{Li}_6\text{PS}_5\text{Cl}$ solid electrolyte for Li-ion solid state batteries. *Electrochim. Acta* **215**, 93–99 (2016).
 23. Yubuchi, S. *et al.* Quantitative analysis of crystallinity in an argyrodite sulfide-based solid electrolyte synthesized via solution processing. *RSC Adv.* **9**, 14465–14471 (2019).
 24. Zhou, Y. *et al.* Observation of Interfacial Degradation of $\text{Li}_6\text{PS}_5\text{Cl}$ against Lithium Metal and LiCoO_2 via In Situ Electrochemical Raman Microscopy. *Batter. Supercaps* **3**, 647–652 (2020).
 25. Dietrich, C. *et al.* Lithium ion conductivity in $\text{Li}_2\text{S}-\text{P}_2\text{S}_5$ glasses – building units and local structure evolution during the crystallization of superionic conductors Li_3PS_4 , $\text{Li}_7\text{P}_3\text{S}_{11}$ and L. *J. Mater. Chem. A* **5**, 18111–18119 (2017).
 26. Mercier, R., Malugani, J. P., Fahys, B., Douglade, J. & Robert, G. Synthèse, structure cristalline et analyse vibrationnelle de l’hexathiohypodiphosphate de lithium $\text{Li}_4\text{P}_2\text{S}_6$. *J. Solid State Chem.* **43**, 151–162 (1982).
 27. Rao, R. P., Sharma, N., Peterson, V. K. & Adams, S. Formation and conductivity studies of lithium argyrodite solid electrolytes using in-situ neutron diffraction. *Solid State Ionics* **230**, 72–76 (2013).
 28. Schwietert, T. K. *et al.* Clarifying the relationship between redox activity and electrochemical stability in solid electrolytes. *Nat. Mater.* **19**, 428–435 (2020).
 29. Dewald, G. F. *et al.* Experimental assessment of the practical oxidative stability of lithium thiophosphate solid electrolytes. *Chem. Mater.* **31**, 8328–8337 (2019).
 30. Tan, D. H. S. *et al.* Elucidating Reversible Electrochemical Redox of $\text{Li}_6\text{PS}_5\text{Cl}$ Solid Electrolyte. *ACS Energy Lett.* **4**, 2418–2427 (2019).

